The Astrophysical Journal, 932:65 (12pp), 2022 June 10 https://doi.org/10.3847/1538-4357/ac6ddc

Turbulent Cosmic Ray–Mediated Shocks in the Hot Ionized Interstellar Medium

B.-B. Wang[1], G. P. Zank[1,2], L.-L. Zhao[1,2], and L. Adhikari[1,2]
[1] Center for Space Plasma and Aeronomic Research (CSPAR), University of Alabama in Huntsville, Huntsville, AL 35899, USA
[2] Department of Space Science, University of Alabama in Huntsville, Huntsville, AL 35899, USA
Received 2022 March 14; revised 2022 May 3; accepted 2022 May 5; published 2022 June 16

Abstract

The structure of shocks and turbulence are strongly modified during the acceleration of cosmic rays (CRs) at a shock wave. The pressure and the collisionless viscous stress decelerate the incoming thermal gas and thus modify the shock structure. A CR streaming instability ahead of the shock generates the turbulence on which CRs scatter. The turbulent magnetic field in turn determines the CR diffusion coefficient and further affects the CR energy spectrum and pressure distribution. The dissipation of turbulence contributes to heating the thermal gas. Within a multicomponent fluid framework, CRs and thermal gas are treated as fluids and are closely coupled to the turbulence. The system equations comprise the gas dynamic equations, the CR pressure evolution equation, and the turbulence transport equations, and we adopt typical parameters for the hot ionized interstellar medium. It is shown that the shock has no discontinuity but possesses a narrow but smooth transition. The self-generated turbulent magnetic field is much stronger than both the large-scale magnetic field and the preexisting turbulent magnetic field. The resulting CR diffusion coefficient is substantially suppressed and is more than three orders smaller near the shock than it is far upstream. The results are qualitatively consistent with certain observations.

Unified Astronomy Thesaurus concepts: Cosmic rays (329); Shocks (2086)

1. Introduction

The acceleration of cosmic rays (CRs) can strongly modify the structure of magnetohydrodynamic (MHD) shocks, typically producing high levels of low-frequency magnetic turbulence that is necessary to scatter CRs back and forth across the shock. Drury & Völk (1981) and Axford et al. (1982) introduced the now classic two-fluid model that comprises a distinct thermal gas and a CR component to determine the structure of a CR-mediated shock. The CRs are treated analogously to an electron fluid, contributing a pressure and energy density and neglecting their tenuous number density. One significant drawback of the simple two-fluid CR models is their apparent efficiency in energizing CRs, with, in some cases, as much as 98% of the upstream kinetic energy being converted into CR energy/pressure and correspondingly almost no downstream heating of the shocked thermal gas. It was suggested that energetic upstream CRs streaming away from the shock front could excite Alfvén waves (Bell 1978) that would enhance the scattering of CRs and thus trap energetic particles in the vicinity of the shock. McKenzie & Völk (1982) recognized that self-generated turbulence might not only be important for particle scattering but could both limit the efficiency of the shock in converting kinetic energy to CR energy and provide a channel for the dissipation of turbulence to heat the downstream plasma. Accordingly, McKenzie & Völk (1982) further included self-excited and preexisting Alfvén waves as a third component of the two-fluid CR model and introduced a hydrodynamic version of the gyroresonant streaming instability as the upstream source of Alfvén waves. The transport of Alfvén waves was treated on the basis of a simple WKB approximation that describes the linear propagation of small-amplitude noninteracting waves and neglects possible mixing and coupling between propagating modes: that is, it was not a turbulence description and hence does not lead to dissipation. The WKB-modified two-fluid model yielded a shock structure that was either completely smoothed or required a subshock to affect the downstream transition. Several reviews provide an excellent introduction to CR-mediated shock structure (Drury 1983; Blandford & Eichler 1987; Jones & Ellison 1991; Malkov & Drury 2001; Blasi 2013).

By using a collisionless Chapman–Enskog expansion, Zank et al. (2014) and Zank (2016) developed a general framework for studying a multicomponent plasma comprising thermal electrons and protons and energetic particles. The presence of energetic particles introduces not only an isotropic pressure but also a viscous stress tensor into the dynamical equations describing the multicomponent gas. The reduced form of the model is structurally similar to the classical CR two-fluid model. The model has been applied to study shock structure in the very local interstellar medium (Zank 2016; Mostafavi et al. 2017; Mostafavi & Zank 2018), a pickup ion (and anomalous CR) mediated heliospheric termination shock (Mostafavi et al. 2017, 2018; Zank et al. 2018), and shock waves in the inner heliosheath (Mostafavi et al. 2019). These models found that the presence of energetic particle viscosity eliminates the need for a gas subshock and all shock transitions from the upstream state to the downstream state are smooth.

Zank et al. (2012) derived a set of transport equations for incompressible MHD turbulence in high-plasma beta inhomogeneous magnetized flows with arbitrarily strong fluctuating fields. On introducing several significant assumptions, the coupled transport equations can be simplified to recover the standard WKB approximation for the transport of Alfvén waves (Zank et al. 2012). The turbulence transport model has been tested successfully against several sets of solar wind observations (Adhikari et al. 2015; Shiota et al. 2017). In this work, we extend the multicomponent fluid model of Zank et al. (2014) by incorporating in closed form the turbulence transport

model of Zank et al. (2012). As noted, the turbulence model is appropriate to a high-plasma beta regime (Zank & Matthaeus 1993; Zank et al. 2017), ensuring that the model derived here is appropriate to the hot interstellar medium. The turbulence is driven primarily by the streaming of CRs (as well as the possible presence of preexisting turbulence), and in turn the CR diffusion coefficient is determined by the turbulent magnetic energy density and the correlation length of magnetic field fluctuations (Zank et al. 1998, 2004; Webb et al. 2006; Zhao et al. 2017, 2018). The dissipation of turbulence heats the thermal gas and increases the thermal gas pressure.

Our purpose is to investigate in detail the role of low-frequency turbulence in determining the structure and properties of CR-mediated shocks, going well beyond the simple WKB description of waves utilized by McKenzie & Völk (1982). We restrict our attention to shock waves that do not exceed the threshold speed above which the nonresonant CR-driven instability identified by Bell (2004) emerges. We present and solve the coupled one-dimensional steady-state fluid equations and turbulence transport equations to investigate shock structure and the evolution of various physical quantities, such as the thermal gas and CR pressure, the total turbulence energy, the cross helicity, the residual energy, the turbulent magnetic field and velocity field energy intensities, the correlation length of the magnetic and velocity field fluctuations, and the CR diffusion coefficient.

2. Governing Equations

We review the basic equations for the coupled thermal plasma, energetic particles, and turbulence and then introduce the boundary conditions for the far upstream state.

2.1. Fluid Equations

Zank et al. (2014) and Zank (2016) developed the model that couples thermal plasma and energetic particles. Here we restrict attention to a flow parallel to the ambient magnetic field, that is, along the x-direction. The reduction of the full multifluid description can be expressed as an MHD-like system of equations. Incorporating the heating due to the dissipation of low-frequency MHD turbulence, the coupled fluid equations can be expressed as

$$\frac{\partial \rho}{\partial t} + \frac{\partial (\rho U)}{\partial x} = 0; \tag{1}$$

$$\rho\left(\frac{\partial U}{\partial t} + U\frac{\partial U}{\partial x}\right) = -\frac{\partial P_g}{\partial x} - \frac{\partial P_c}{\partial x} - \frac{\partial \Pi}{\partial x} - \frac{\partial P_w}{\partial x}; \tag{2}$$

$$\frac{\partial P_g}{\partial t} + U\frac{\partial P_g}{\partial x} + \gamma_g P_g \frac{\partial U}{\partial x} = (\gamma_g - 1)\frac{\rho}{2\lambda} \times [(E_T + E_C)(E_T - E_C)^{1/2} + (E_T - E_C)(E_T + E_C)^{1/2}]; \tag{3}$$

$$\frac{\partial P_c}{\partial t} + (U - \sigma_C V_A)\frac{\partial P_c}{\partial x} + \gamma_c P_c \frac{\partial}{\partial x}(U - \sigma_C V_A) = \frac{1}{3}\frac{\partial}{\partial x}\left(K\frac{\partial P_c}{\partial x}\right) - (\gamma_c - 1)\Pi\frac{\partial}{\partial x}(U - \sigma_C V_A); \tag{4}$$

$$\frac{\partial}{\partial t}\left(\frac{1}{2}\rho U^2 + \frac{\gamma_c P_c}{\gamma_c - 1} + \frac{\gamma_g P_g}{\gamma_g - 1} + E_w\right) + \frac{\partial}{\partial x}\left(\frac{1}{2}\rho U^2 U + \frac{\gamma_c}{\gamma_c - 1}P_c(U - \sigma_C V_A) + \frac{\gamma_g P_g}{\gamma_g - 1}U + \Pi(U - \sigma_C V_A) - \frac{1}{\gamma_c - 1}\frac{K}{3}\frac{dP_c}{dx} + (U - \sigma_C V_A)E_w + UP_w\right) = 0, \tag{5}$$

where U is the gas flow velocity, V_A is the Alfvén speed, P_g is the thermal gas pressure, P_c is the CR pressure, E_w is the turbulence energy density, P_w is the turbulence pressure, K is the energy-averaged diffusion coefficient, $\gamma_g = 5/3$ is the adiabatic index for gas, $\gamma_c = 4/3$ is the adiabatic index for CRs, E_T is the total turbulence energy, E_C is the cross helicity ($\sigma_C = E_C/E_T$), and λ is the correlation length. The CR stress tensor resulting from the effect of viscosity is expressed as $\Pi = -\frac{4}{45}\eta(dU/dx)$, where η is the coefficient of collisionless viscosity and can be approximated as $\eta \approx P_c\tau_s$ (τ_s is the turbulence-particle scattering time). As illustrated by the right-hand side of Equation (3), the dissipation of turbulence heats the thermal gas. The heating rate is controlled by the correlation length λ, the total turbulence energy density E_T, and the cross helicity E_C.

Since the energy dependence of the spatial diffusion coefficient D (where D is the kinetic form of the spatial diffusion coefficient and not the energy-averaged form K used in Equation (5)) is weak, the energy-averaged diffusion coefficient K is not too different from D for energetic particles of mean energy (Zweibel 2017). By way of simplification, we take the spatial part of D as a first approximation for K. Here we adopt the spatial diffusion coefficient derived by Zank et al. (1998) using a quasilinear theory approach. We assume a uniform magnetic field B parallel to the flow direction and a turbulent magnetic field with a Kolmogorov power spectrum. For the case when particle gyroradii R_L are much smaller than the correlation length of magnetic field fluctuations λ, the mean free path l is given by

$$l = 3.1371\frac{B^{5/3}}{\langle \delta B_x^2\rangle}\left(\frac{P}{c}\right)^{1/3}\lambda^{2/3} = 3.2186 \times 10^{-2}\frac{B^2}{\langle \delta B_x^2\rangle}\left(\frac{1\ \mu\mathrm{G}}{B}\right)^{1/3} \times \left(\frac{p}{1\ \mathrm{GeV}/c}\right)^{1/3}\left(\frac{\lambda}{1\ \mathrm{pc}}\right)^{2/3}\ \mathrm{pc}, \tag{6}$$

where $\delta B = 2\delta B_x$ is the turbulence magnetic field at the injection scale, P is the CR particle rigidity, c is the speed of light, p is the CR particle momentum, and λ is the correlation length for the magnetic field fluctuations. The diffusion coefficient D may be expressed as

$$D \equiv \frac{vl}{3} = k_0 k_x(x) k_p(p); \tag{7}$$

$$k_p(p) = \beta\left(\frac{p}{1\ \mathrm{GeV}\ c^{-1}}\right)^{1/3}; \tag{8}$$

$$k_x(x) = \frac{\langle \delta B_x^2(0)\rangle}{\langle \delta B_x^2(x)\rangle}\left(\frac{\lambda(x)}{\lambda(0)}\right)^{2/3}; \quad (9)$$

$$k_0 = 9.9316 \times 10^{26}\mathrm{cm^2\ s^{-1}}\frac{B^2}{\langle \delta B_x^2(0)\rangle}\left(\frac{1\ \mu\mathrm{G}}{B}\right)^{1/3}\left(\frac{\lambda(0)}{1\ \mathrm{pc}}\right)^{2/3}, \quad (10)$$

where β is the particle speed v in units of the speed of light. The diffusion coefficient and turbulence-particle scattering time are related through $D = v^2\tau_s/3$. The diffusion coefficient is composed of three components: the constant number k_0, the spatially dependent part $k_x(x)$, and the momentum-dependent part $k_p(p)$. The quasilinear transport model is based on the essential assumption that the fluctuating magnetic field is weak, that is, $\delta B \ll B$. It is possible that the amplification of turbulence by CRs could invalidate this assumption. However, test particle simulations with a Kolmogorov MHD turbulence spectrum, assumed slab geometry, and relatively low energy particles (i.e., $R_L/\lambda \ll 1$) show that the quasilinear transport model is in rough agreement even for large values of $\delta B/B$. For example, Shalchi (2009) assumes $R_L/\lambda \approx 0.13$ and $\delta B/B \approx 20$, finding that test particle simulation results are in reasonable agreement with quasilinear theory, as are test particle simulations by Snodin et al. (2016), for high turbulence levels provided $R_L/\lambda \ll 1$. Minnie et al. (2007) simulated the charged-particle transport in a composite (slab+2D) turbulence and showed that the quasilinear transport model still yields reasonable estimates for the parallel mean free path at low or intermediate turbulence levels.

2.2. Turbulence Transport Equations

The turbulence transport model developed by Zank et al. (2012) describes the evolution of turbulence energy, the cross helicity, the residual energy, and the associated correlation lengths in the large plasma beta limit. These six coupled equations can be reduced to four by using a single correlation length approximation (Dosch et al. 2013) to describe the interaction of turbulence with parallel and perpendicular shocks (Adhikari et al. 2016). We adopt the reduced turbulence model with four coupled equations and introduce the CR streaming instability as the source of turbulence. It can be shown that (McKenzie & Völk 1982) the CR streaming instability (Lerche 1967) is proportional to $V_A(\partial P_c/\partial x)$. We also include the term associated with CR viscosity in the source, although this term is ignored in the computation for simplification. The turbulence transport equations have the form:

$$\begin{aligned}&\frac{\partial E_T}{\partial t} + U\frac{\partial E_T}{\partial x} - V_A\frac{\partial E_C}{\partial x} + \frac{\partial U}{\partial x}\\ &\times\left[\frac{E_T}{2} + \left(2a - \frac{1}{2}\right)E_D\right] + \frac{\partial V_A}{\partial x}E_C\\ &= -\left[\frac{(E_T + E_C)(E_T - E_C)^{1/2}}{\lambda} + \frac{(E_T - E_C)(E_T + E_C)^{1/2}}{\lambda}\right]\\ &+ \frac{2}{\rho}\sigma_C V_A\left(\frac{\partial P_c}{\partial x} + \frac{\partial \Pi}{\partial x}\right);\end{aligned} \quad (11)$$

$$\begin{aligned}&\frac{\partial E_C}{\partial t} + U\frac{\partial E_C}{\partial x} - V_A\frac{\partial E_T}{\partial x} + \frac{\partial U}{\partial x}\frac{E_C}{2} + \frac{\partial V_A}{\partial x}E_T - \frac{\partial V_A}{\partial x}E_D\\ &= -\left[\frac{(E_T + E_C)(E_T - E_C)^{1/2}}{\lambda}\right)\\ &-\frac{(E_T - E_C)(E_T + E_C)^{1/2}}{\lambda}\Bigg]\\ &+ \frac{2}{\rho}\sigma_C V_A\left(\frac{\partial P_c}{\partial x} + \frac{\partial \Pi}{\partial x}\right);\end{aligned} \quad (12)$$

$$\begin{aligned}&\frac{\partial E_D}{\partial t} + U\frac{\partial E_D}{\partial x} + \frac{1}{2}\frac{\partial U}{\partial x}\left[\left(2a - \frac{1}{2}\right)2E_T + E_D\right]\\ &+ \frac{V_A}{\sqrt{E_T^2 - E_C^2}}\left[E_C\frac{\partial E_T}{\partial x} - E_T\frac{\partial E_C}{\partial x}\right]\\ &+ \frac{\partial V_A}{\partial x}E_C = -E_D\left[\frac{(E_T + E_C)^{1/2} + (E_T - E_C)^{1/2}}{\lambda}\right];\end{aligned} \quad (13)$$

$$\begin{aligned}&\frac{\partial \lambda}{\partial t} + U\frac{\partial \lambda}{\partial x} = (E_T + E_C)^{1/2} + (E_T - E_C)^{1/2}\\ &- \frac{\lambda}{E_T + E_C}\frac{2}{\rho}\sigma_C V_A\left(\frac{\partial P_c}{\partial x} + \frac{\partial \Pi}{\partial x}\right),\end{aligned} \quad (14)$$

where E_T is twice the sum of turbulent kinetic energy density and magnetic energy density per unit mass (often called the turbulence energy for convenience), and E_C is the cross helicity, which is half the energy difference between the backward and forward propagating modes. The direction is relative to the background large-scale magnetic field direction in the shock frame. E_D is the residual energy, which is twice the difference between the turbulent kinetic energy and the turbulent magnetic energy, and λ is the correlation length. In the reduced turbulence transport equation, the correlation lengths for the forward propagating mode and that for the backward mode are the same and equal to one half the correlation length for the residual energy. In this case, the correlation length of the magnetic field fluctuations is simplified to λ (Zank et al. 2012; Dosch et al. 2013; Zank et al. 2017). The turbulent energy and cross-helicity are related to the Elsässer variables $\boldsymbol{z}^{\pm} \equiv \boldsymbol{u} \pm \boldsymbol{b}/\sqrt{\mu_0\rho}$, where $\boldsymbol{u}$ and $\boldsymbol{b}$ are the fluctuating velocity and magnetic fields and ρ is the nonfluctuating mass density. We may then express the turbulent energy and cross-helicity as

$$\begin{aligned}&\langle z^{+2}\rangle = E_T + E_C; \qquad \langle z^{-2}\rangle = E_T - E_C;\\ &E_D = \langle \boldsymbol{z}^+ \cdot \boldsymbol{z}^-\rangle = \langle u^2\rangle - \langle b^2\rangle/(\mu_0\rho);\end{aligned} \quad (15)$$

$$\sigma_C = \frac{E_C}{E_T}; \qquad \sigma_D = \frac{E_D}{E_T}, \quad (16)$$

where σ_C is the normalized cross helicity and σ_D is the normalized residual energy.

We have shown that the transport equation for the turbulence energy density $E_w = \rho/2E_T$ can be expressed in a conservative form through the introduction of a generalized pressure tensor (Wang et al. 2021). The evolution equation of the turbulence energy density E_w, without specifying the source term, is given

by Wang et al. (2021):

$$\frac{\partial E_w}{\partial t} + \nabla \cdot [(\boldsymbol{U} - \sigma_C \boldsymbol{V}_A)E_w + \boldsymbol{U} \cdot \boldsymbol{P}_w] = \boldsymbol{U} \cdot \nabla \cdot \boldsymbol{P}_w - \frac{\rho}{2}\left[\frac{(E_T + E_C)(E_T - E_C)^{1/2} - (E_T - E_C)(E_T + E_C)^{1/2}}{\lambda}\right], \quad (17)$$

and the turbulence pressure tensor can be expressed as

$$\begin{aligned}\boldsymbol{P}_w &= \left[\frac{E_w}{2} + (2a - \frac{1}{2})\sigma_D E_w\right]\boldsymbol{I} - 2a\sigma_D E_w \Gamma\boldsymbol{\Gamma} \\ &= \left[a\rho\langle \boldsymbol{u}^2\rangle + (1 - 2a)\frac{\langle \boldsymbol{b}^2\rangle}{8\pi}\right]\boldsymbol{I} \\ &\quad - a\left(\rho\langle \boldsymbol{u}^2\rangle - \frac{\langle \boldsymbol{b}^2\rangle}{4\pi}\right)\Gamma\boldsymbol{\Gamma}, \end{aligned} \quad (18)$$

where a is a structural similarity parameter and n corresponds to a specified direction for axisymmetric turbulence. The evolution equation resembles formally the well-known WKB transport equation for the energy density of linear Alfvén waves in an inhomogeneous flow. However, unlike the WKB model, the turbulence energy propagates with the speed $\sigma_C V_A$. The energy density flux in the turbulence conservation law contains the cross helicity. The cross helicity is governed by an independent turbulence transport equation that must be solved in conjunction with the energy transport equation. The turbulence pressure tensor $\boldsymbol{P}_w$ is also different from the wave pressure tensor of the WKB model, involving both the energy densities of the fluctuating velocity and magnetic fields. The relevant anisotropies of the underlying turbulence are also included in the turbulence pressure tensors as expressed through the structural similarity parameter a. Finally, the dissipation of turbulence is properly incorporated in the conservation laws and is based on a Kolmogorov formalism. For the 3D isotropic turbulence used in this work, $a = 1/3$ and $\boldsymbol{n} = 0$, implying that the corresponding turbulence pressure tensor reduces to

$$\boldsymbol{P}_w = \frac{\rho}{4}(E_T + \frac{1}{3}E_D)\boldsymbol{I} = (\gamma_w - 1)E_w\boldsymbol{I}, \quad (19)$$

where $\gamma_w = \frac{3}{2} + \frac{\sigma_D}{6}$ is the "adiabatic index" for turbulence. For Alfvén-like turbulence with $E_D = 0 = \sigma_D$ (as in the WKB model), the turbulence pressure reverts to the isotropic Alfvén wave pressure form $\langle \boldsymbol{b}^2\rangle/(8\pi)I$ and $\gamma_w = 3/2$. In our initial investigations below, we neglect the turbulence pressure/energy contribution in the calculation, checking its post facto magnitude for consistency.

In this work, we assume that the gyroresonant streaming instability is the only source of turbulence, neglecting preexisting interstellar turbulence. The nonresonant instability found by Bell (2004) is present only when the shock speed $U \geqslant \mathcal{O}(3(V_A^2 c)^{1/3})$ (Amato & Blasi 2009). For smaller shock speeds, the nonresonant mode disappears and only the resonant mechanism can amplify the turbulence (Amato & Blasi 2009). Implicit in the transport Equations (11)–(14) is that the turbulence is fully developed and governed by the Kolmogorov theory (or Iroshnikov–Kraichnan theory) for which the injection of energy at the inertial range is balanced by the rate of dissipation (Zank et al. 2012). This assumption yields the form of the dissipation terms on the right-hand sides of Equations (11)–(14). This approach also has the considerable benefit of not needing to identify precise damping mechanisms since the turbulent fluctuations cascade nonlinearly from small wavenumbers to high wavenumbers, where dissipation then "drains" the fluctuating energy at the smallest or dissipation scale, which results in heating of the thermal plasma. One important distinction for the cascade picture is the possibility that turbulence may be damped due to collisions between ions and neutrals in the gas, since this opens an alternate path for energy transfer. However, for the hot ionized medium, the gas is completely ionized, allowing us to neglect ion-neutral damping. Nonlinear Landau damping, caused by resonate interactions between thermal ions and an acoustic beat wave formed by two interfering Alfvén waves, only operates efficiently when the damping length is much smaller than the diffusion convection length (Völk et al. 1984). This condition requires that the shock speed satisfy $U \geqslant \sqrt{c v_{\rm th}/2} \approx 1356 \times (T/10^4{\rm K})^{1/4}$ km s^{-1} ($v_{\rm th}$ is the gas thermal speed). We consider a shock speed of 3000 km s^{-1} in the far upstream with a gas temperature of 10^6 K, ensuring that nonlinear Landau damping is unlikely to be an efficient damping mechanism in the far upstream, and for simplification, we therefore neglect nonlinear Landau damping.

We normalize Equations (1)–(5) and (11)–(14) with respect to typical fixed parameters that represent characteristic far upstream values using

$$\bar{x} = x/A, \qquad \bar{P}_g = P_g/P_{g0}, \qquad \bar{P}_c = P_c/P_{g0}, \qquad \bar{E}_T = E_T/U_0^2, \quad (20)$$

$$\bar{E}_C = E_C/U_0^2, \qquad \bar{E}_D = E_D/U_0^2, \qquad \bar{\lambda} = \lambda/A, \quad (21)$$

where $A = 1$ pc and the subscript 0 indicates the far upstream state. Note that we normalize the distance x to a fixed 1 pc rather than the characteristic scale k_0/U_0, which is too large compared with the shock width. The steady normalized coupled equations can be expressed as

$$\begin{aligned}\overline{U}\frac{d\overline{E}_T}{d\bar{x}} - \frac{\overline{V}_A}{M_{A0}}\frac{d\overline{E}_c}{d\bar{x}} + \frac{d\overline{U}}{d\bar{x}}\left(\frac{\overline{E}_T}{2} + (2a - \frac{1}{2})\overline{E}_D\right) + \frac{\overline{E}_C}{M_{A0}}\frac{d\overline{V}_A}{d\bar{x}} \\ = -\frac{1}{\bar{\lambda}}\overline{E}_T + \overline{E}_C\overline{E}_T - \overline{E}_C{}^{1/2} \\ +(\overline{E}_T - \overline{E}_C)\overline{E}_T + \overline{E}_C{}^{1/2} \\ + \frac{2\overline{U}\overline{V}_A\sigma_C}{\gamma_g M_{S0}^2 M_{A0}}\frac{d\overline{P}_c}{d\bar{x}}; \end{aligned} \quad (22)$$

$$\begin{aligned}\overline{U}\frac{d\overline{E}_C}{d\bar{x}} - \frac{\overline{V}_A}{M_{A0}}\frac{d\overline{E}_T}{d\bar{x}} + \frac{\overline{E}_C}{2}\frac{d\overline{U}}{d\bar{x}} + \frac{\overline{E}_T - \overline{E}_D}{M_{A0}}\frac{d\overline{V}_A}{d\bar{x}} \\ = -\frac{1}{\bar{\lambda}}(\overline{E}_T + \overline{E}_C)\overline{E}_T - \overline{E}_C{}^{1/2} - (\overline{E}_T - \overline{E}_C)\overline{E}_T + \overline{E}_C{}^{1/2} \\ + \frac{2\overline{U}\overline{V}_A\sigma_C}{\gamma_g M_{S0}^2 M_{A0}}\frac{d\overline{P}_c}{d\bar{x}}; \end{aligned} \quad (23)$$

$$\overline{U}\frac{d\overline{E}_D}{d\overline{x}} + \frac{1}{2}\frac{d\overline{U}}{d\overline{x}}[2(2a-1/2)\overline{E}_T + \overline{E}_D] + \frac{\overline{V}_A}{M_{A0}}\left[\overline{E}_C\frac{d\overline{E}_T}{d\overline{x}} - \overline{E}_T\frac{d\overline{E}_C}{d\overline{x}}\right]/\sqrt{\overline{E}_T{}^2 - \overline{E}_C{}^2} + \frac{\overline{E}_C}{M_{A0}}\frac{d\overline{V}_A}{d\overline{x}} = -\frac{1}{\overline{\lambda}}\overline{E}_D[(\overline{E}_T + \overline{E}_C)^{1/2} + (\overline{E}_T - \overline{E}_C)^{1/2}]; \quad (24)$$

$$\overline{U}\frac{d\overline{\lambda}}{d\overline{x}} = (\overline{E}_T + \overline{E}_C)^{1/2} +](\overline{E}_T - \overline{E}_C)^{1/2} - \frac{2\overline{\lambda}}{\gamma_g M_{S0}^2 M_{A0}}\frac{\overline{U}\overline{V}_A\sigma_C}{\overline{E}_T + \overline{E}_C}\frac{d\overline{P}_C}{d\overline{x}} \quad (25)$$

$$\bar{U}\frac{d\bar{P}_g}{d\bar{x}} = (\gamma_g - 1)\frac{\gamma_g M_{S0}^2}{2\bar{\lambda}\bar{U}}[(\bar{E}_T + \bar{E}_C)(\bar{E}_T - \bar{E}_C)^{1/2} + (\bar{E}_T - \bar{E}_C)(\bar{E}_T + \bar{E}_C)^{1/2}] - \gamma_g\bar{P}_g\frac{d\bar{U}}{d\bar{x}}; \quad (26)$$

$$\frac{1}{3(\gamma_c - 1)}\frac{d\overline{P}_c}{d\overline{x}} = \left[\frac{\gamma_g}{2}M_{S0}^2(\overline{U}^2 - 1) + \frac{\gamma_c}{\gamma_c - 1}\left(\overline{P}_c\,\overline{U} - \frac{P_{c0}}{P_{g0}} - (\sigma_C\,\overline{V}_A\overline{P}_c - \sigma_{C0}\frac{P_{c0}}{P_{g0}})/M_{A0}\right) + \frac{\gamma_g}{\gamma_g - 1}(\overline{P}_g U - 1)\right]\left(\frac{A}{k_0 k_x(x)/U_0}\right) - \frac{4}{15}\left(\overline{U} - \sigma_C\frac{\overline{V}_A}{M_{A0}}\right)\overline{P}_c\left(\frac{U_0}{c}\right)^2\frac{d\overline{U}}{d\overline{x}}; \quad (27)$$

$$\frac{4}{15}\frac{d\bar{U}}{d\bar{x}} = [\gamma_g M_{S0}^2(\bar{U} - 1) + (\bar{P}_g - 1) + (\bar{P}_c - \frac{P_{c0}}{P_{g0}})]\frac{A}{k_0 k_x(x)/U_0\bar{P}_c}\left(\frac{U_0}{c}\right)^{-2}, \quad (28)$$

where M_{S0} and M_{A0} are the far upstream sonic Mach number and Alfvén Mach number, respectively.

2.3. Far Upstream Boundary Conditions

The far upstream state is determined by the following quantities: $\bar{U}_0 = 1$, $\bar{P}_{g0} = 1$, $\bar{P}_{c0} = 0.01$, M_{S0}, M_{A0}, $\bar{E}_{T0}$, $\bar{E}_{c0}$, $\bar{E}_{D0}$, $\bar{\lambda}_0$. We present a brief discussion about typical quantities for the hot ionized interstellar medium.

The sound speed in the hot ionized medium is given by

$$C_s = \sqrt{\frac{\gamma_g 2k_B T}{m}} = 128.5\left(\frac{\gamma_g T}{K}\right)^{1/2}\left(\frac{m}{m_p}\right)^{-1/2}\ \mathrm{m\ s^{-1}}, \quad (29)$$

where k_B is the Boltzmann constant, T is the gas temperature in units of Kelvin, m is the gas mean mass ($m \approx 1.4 m_p$), and m_p is the proton mass. For a gas with temperature 10^6 K, the sound speed is about 140 km s^{-1} and the sonic Mach number $M_{S0} = U_0/C_S$ is about 21.4 for a shock speed of 3000 km s^{-1}.

The Alfvén speed is determined by both the large-scale magnetic field strength B and the ion density n_i,

$$V_A = \frac{B}{\sqrt{\mu_0\rho_i}} = 2.18\frac{B}{\mu\mathrm{G}}\left(\frac{n_i}{\mathrm{cm^{-3}}}\right)^{-1/2}\left(\frac{m}{m_p}\right)^{-1/2}\ \mathrm{km\ s^{-1}}. \quad (30)$$

For a typical magnetic field of about 5 μG in the interstellar medium, and a hot ionized gas with number density of 0.01 cm^{-3}, the Alfvén speed is 92 km s^{-1}. The corresponding Alfvén Mach number $M_{A0} = U_0/V_A$ is 32.6 for the speed shock of 3000 km s^{-1}.

$\bar{E}_{T0}$ is the normalized total turbulence energy in the far upstream. It is assumed that the turbulent kinetic energy and turbulent magnetic energy are in a state of near equipartition in the interstellar medium (Zweibel & McKee 1995; Beck et al. 1996; Minter & Spangler 1997). Thus, $\bar{E}_{D0} \approx 0$ and $\bar{E}_{T0}$ can be estimated as

$$\overline{E}_{T0} = (\langle\delta U^2\rangle + \langle\delta B^2\rangle/(\mu_0\rho_0))/U_0^2 \approx 2\frac{\langle\delta B^2\rangle}{\mu_0\rho_0}/U_0^2 = 2\frac{\langle\delta B^2\rangle}{B^2}\frac{V_A^2}{U_0^2} = \frac{2}{M_{A0}^2}\frac{\langle\delta B^2\rangle}{B^2}. \quad (31)$$

Based on multifrequency polarimetric observations of the diffuse Galactic synchrotron background in the field of view, the ratio of the random to the regular magnetic field strength is 0.7 ± 0.5 (Haverkorn et al. 2004). An analysis of 23 GHz Wilkinson Microwave Anisotropy Probe polarization data derives a ratio of 0.57 (Miville-Deschênes et al. 2008). In this work, we assume $\langle\delta B^2\rangle/B^2 \approx 0.4$.

The amplitude of the normalized cross helicity $\bar{E}_{C0}$ is less clear. For balanced slab turbulence, that is, with equal intensities in forward and backward Elsässer fluctuations, $\langle z^{+2}\rangle = \langle z^{-2}\rangle$ for which $\bar{E}_{C0}$ is zero. However, balanced fully developed turbulence is infrequently observed in the solar wind (e.g., Zank et al. 2021b; Adhikari et al. 2021), so the assumption $\bar{E}_{C0} \approx 0$ is unlikely to be very accurate, although it should be considered. Since the normalized cross helicity $\sigma_C = E_C/E_T$ and $-1 \leqslant \sigma_C \leqslant 1$, we can write $\bar{E}_{C0} = \sigma_C\bar{E}_{T0}$. We consider two possible choices of normalized cross helicity, $\sigma_C = 0.05$ or $\sigma_C = 0.5$.

The correlation length for magnetic field fluctuations derived from various observations occupies a wide range of values, ~1–100 pc (Haverkorn et al. 2008; Haverkorn & Spangler 2013). Here we deduce an appropriate correlation length using the specified diffusion coefficient. We assume a far upstream CR diffusion coefficient $k_0 = 10^{28}$ cm^2 s^{-1}, which is consistent with that derived from the fitting of recent CR data (Evoli et al. 2019; De La Torre Luque et al. 2021). For $\delta B^2/B^2 = 0.4$ and $B = 5\ \mu$G, we derive a correlation length $\lambda = 2.26$ pc from Equation (10). The far upstream diffusion convection length scale is $k_0/U_0 = 10.8$ pc.

The main model parameters are summarized as follows: $M_{S0} = 21.4$, $M_{A0} = 32.6$, $\bar{E}_{T0} = 0.00075$, $\bar{E}_{C0} = 0.05$ or 0.5, $\bar{E}_{D0} = 0$, $\bar{\lambda} = 2.26$.

3. Results and Discussions

We use the public package DifferentialEquations.jl (Rackauckas & Nie 2017) with the solver CVODE (Hindmarsh et al. 2005) to solve the steady normalized coupled Equations (22)–(28). To solve stiff problems, CVODE uses backward difference formulae in the

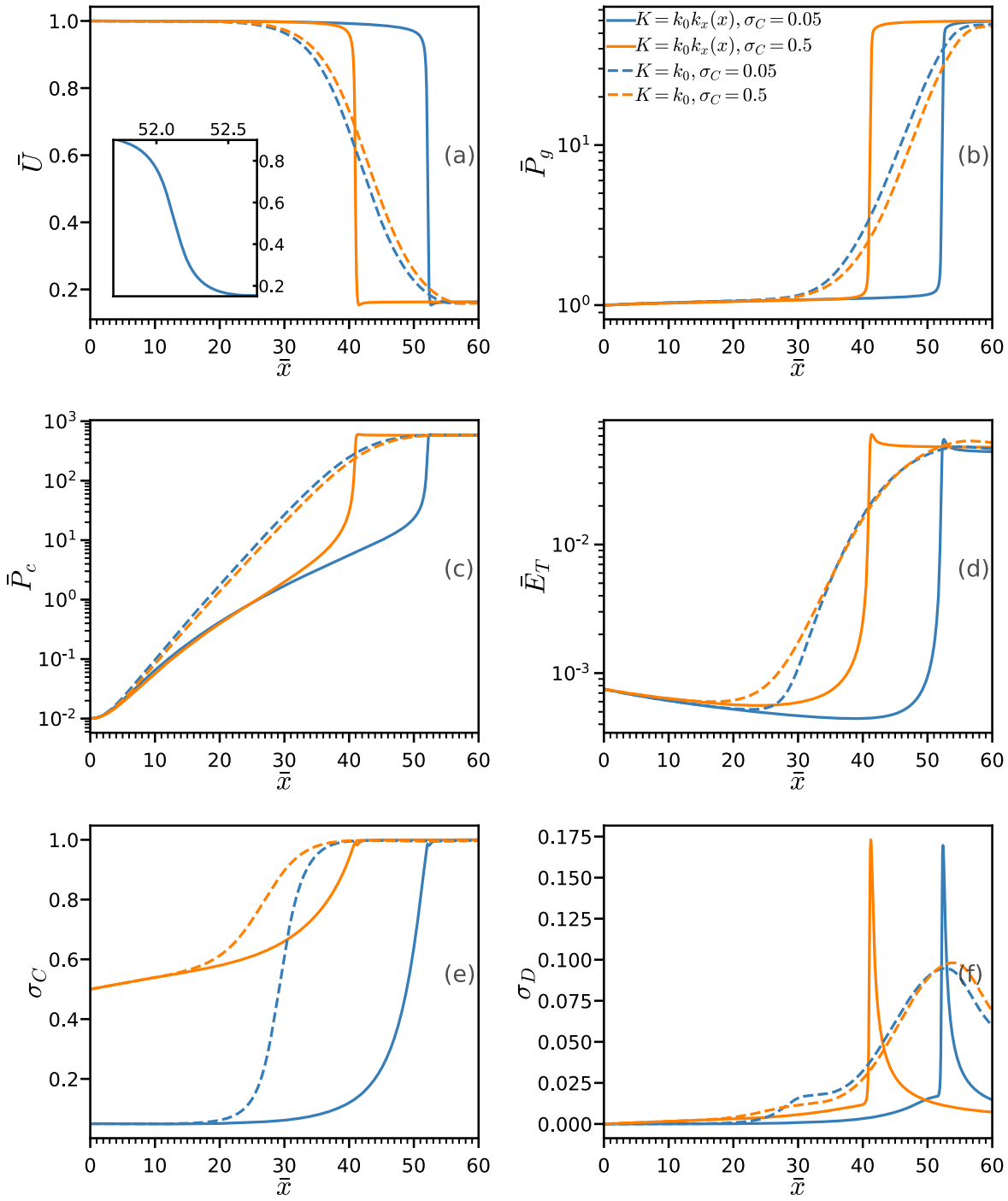

Figure 1. Solutions of the coupled turbulence-CR Equations (22)–(28). The blue (orange) solid lines represent solutions of the model with a spatially dependent diffusion coefficient and $\sigma_C = 0.05$ ($\sigma_C = 0.5$), while the blue (orange) dashed lines correspond to solutions using a constant diffusion coefficient and $\sigma_C = 0.05$ ($\sigma_C = 0.5$). The panels show (*a*) the normalized gas flow speed $\bar{U}$, (*b*) the normalized thermal gas pressure $\bar{P}_g$, (*c*) the normalized CR pressure $\bar{P}_c$, (*d*) the normalized total turbulence energy $\bar{E}_T$, (*e*) the normalized turbulence cross helicity σ_C, and (*f*) the normalized turbulence residual energy σ_D.

so-called fixed-leading coefficient form, with adaptive order between 1 and 5 and adaptive step size.

3.1. Numerical Solutions of the Coupled Turbulence-CR System

The solutions of the coupled Equations (22)–(28) are shown in Figures 1 and 2. The blue (orange) solid lines indicate a model with a self-consistent spatial dependent diffusion coefficient ($K = k_0 k_x$) and $\sigma_C = 0.05$ ($\sigma_C = 0.5$). The blue (orange) dashed lines correspond to solutions with a constant diffusion coefficient $K = k_0$ and $\sigma_C = 0.05$ ($\sigma_C = 0.5$).

We consider first the model solutions that use a spatially dependent CR diffusion coefficient. Thereafter, we compare the results to the constant diffusion coefficient model. Figure 1(a) shows the evolution of the normalized gas speed $\bar{U}$. The gas speed decreases slightly from the far upstream value and is decelerated rapidly in a very narrow region. In the subplot of 1(a) we show the detail of the gas speed profile for the blue solid line. We find that the gas speed decreases from 0.9 to a

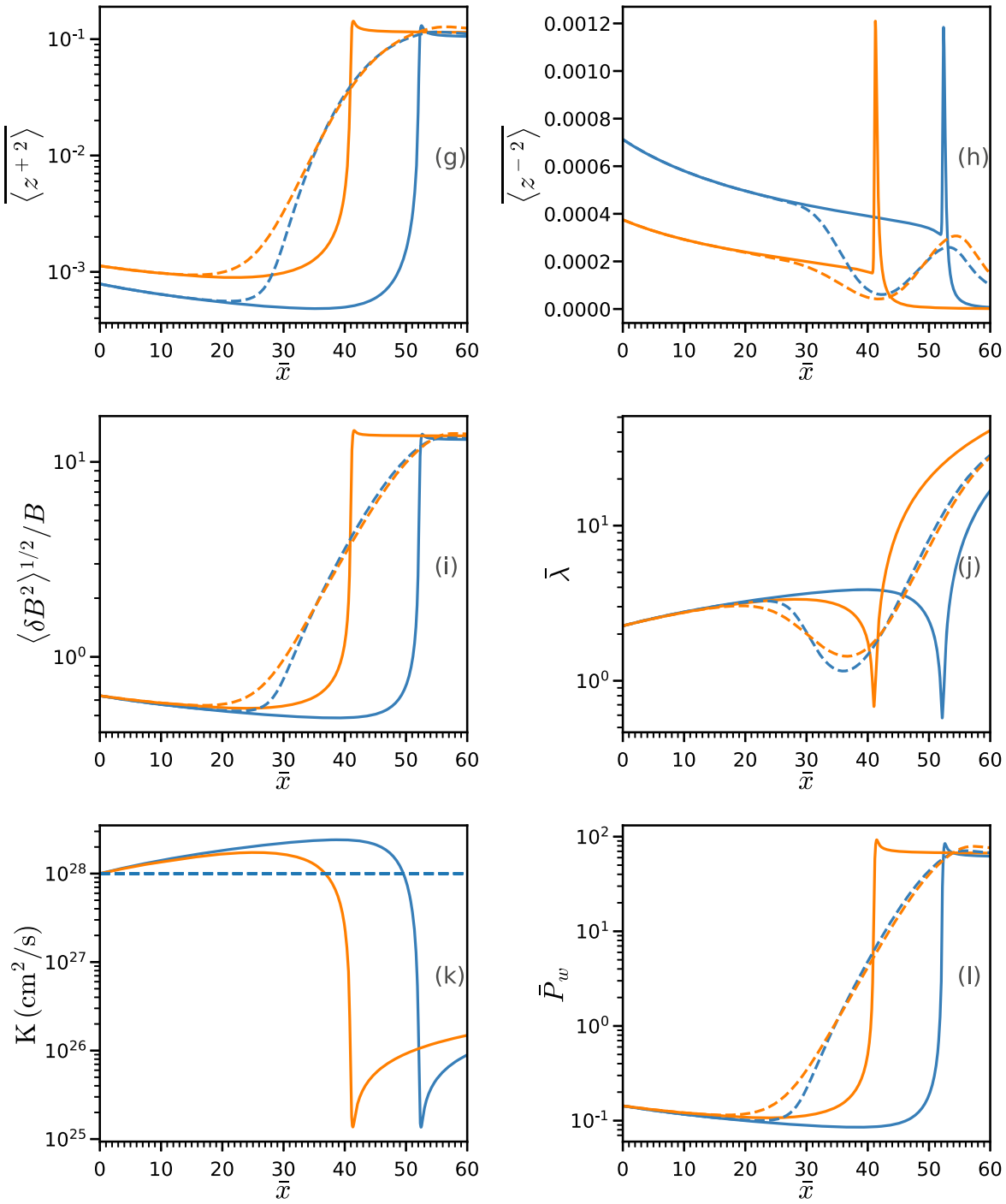

Figure 2. Continuation of Figure 1. The panels show (*g*) the normalized energy in backward propagating modes $\overline{\langle z^{+2}\rangle}$, (*h*) the normalized energy in forward propagating modes $\overline{\langle z^{-2}\rangle}$, (*i*) the magnetic turbulence amplitude $\langle \delta B^2\rangle^{1/2}/B$, (*j*) the normalized correlation length $\bar{\lambda}$, (*k*) the CR diffusion coefficient K, and (*l*) the turbulent pressure.

minimum of 0.153 from $\bar{x} = 51.73$ to $\bar{x} = 52.67$. For the orange line, the corresponding region is from $\bar{x} = 40.61$ to $\bar{x} = 41.54$. Note that $\Delta x = \Delta\bar{x} \times 1$ pc, making the shock width ∼0.9 pc. The quick decrease is followed by a very slight and slow increase, and the speed reaches a terminal speed far downstream.

Figure 1(b) shows the change in normalized gas pressure $\bar{P}_g$, which increases very slowly from the far upstream value, and then increases significantly in the transition region. Immediately after the shock, the gas pressure continues to increase as turbulence generated upstream and amplified in the shock is dissipated downstream. Far downstream, as the turbulence is largely dissipated, the resulting growth in gas pressure is negligible.

The evolution of the normalized CR pressure $\bar{P}_c$ is illustrated in Figure 1(c). Far upstream, the CR pressure is negligibly small and cannot generate turbulence efficiently. However, with the increasing CR pressure upstream, the growth in CR pressure soon outstrips the gas pressure. Upstream of the shock, at $\bar{x} \approx 26$, the CR pressure (both the blue and orange

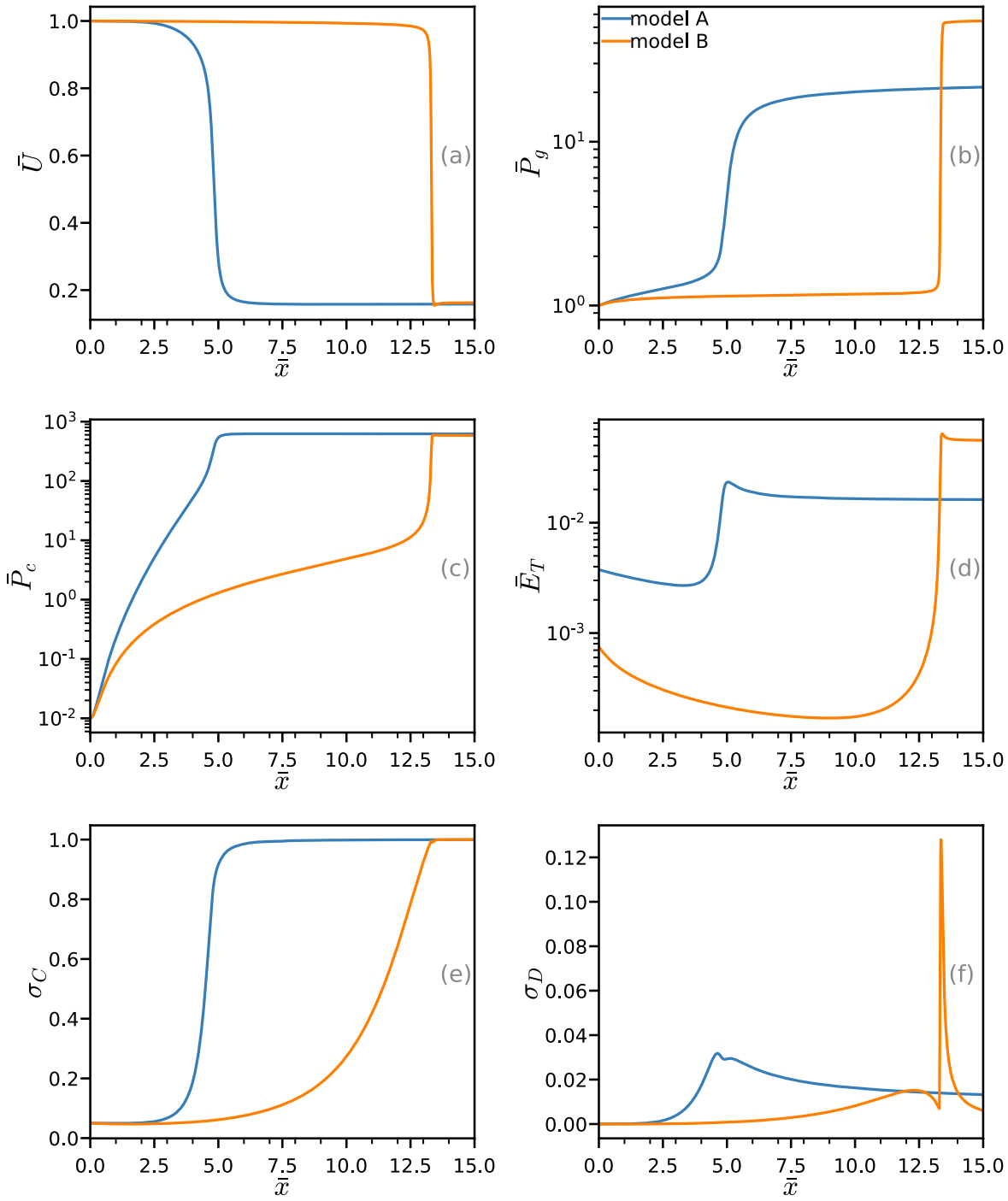

Figure 3. Solutions of the coupled equations with a diffusion coefficient 10^{27} cm^2 s^{-1} far upstream. The blue and orange solid lines represent solutions for models A and B, respectively.

solid lines) exceeds the gas pressure. The maximum CR pressure P_c is about 15 times larger than the gas pressure, making CRs an important dynamical component of the shock that cannot be ignored. Near the shock, the CR pressure gradient is very large and strongly amplifies the turbulence. After the shock, $\bar{P}_c$ decreases slightly and approaches a constant value.

Figure 1(d) shows the variation in the normalized turbulence energy $\bar{E}_T$. From far upstream, the total turbulence energy decreases gradually with increasing distance as the turbulence dissipates. At $\bar{x} = 38.6$ ($\bar{x} = 24.0$) for the blue (orange) solid line, $\bar{E}_T$ reaches a minimum. Thereafter, as the CR streaming instability strengthens as the gradient in the CR pressure increases, the turbulence energy grows rapidly to a maximum immediately downstream of the shock. Thanks to the strong amplification and dissipation of the turbulence, a spike structure around the shock is formed.

As illustrated in Figure 1(e), the normalized cross helicity σ_C changes quite dramatically from the far upstream value; σ_C approaches 1 near the shock and remains at that value downstream of the shock. This is of course a consequence of the CR-streaming-generated turbulence propagating against the

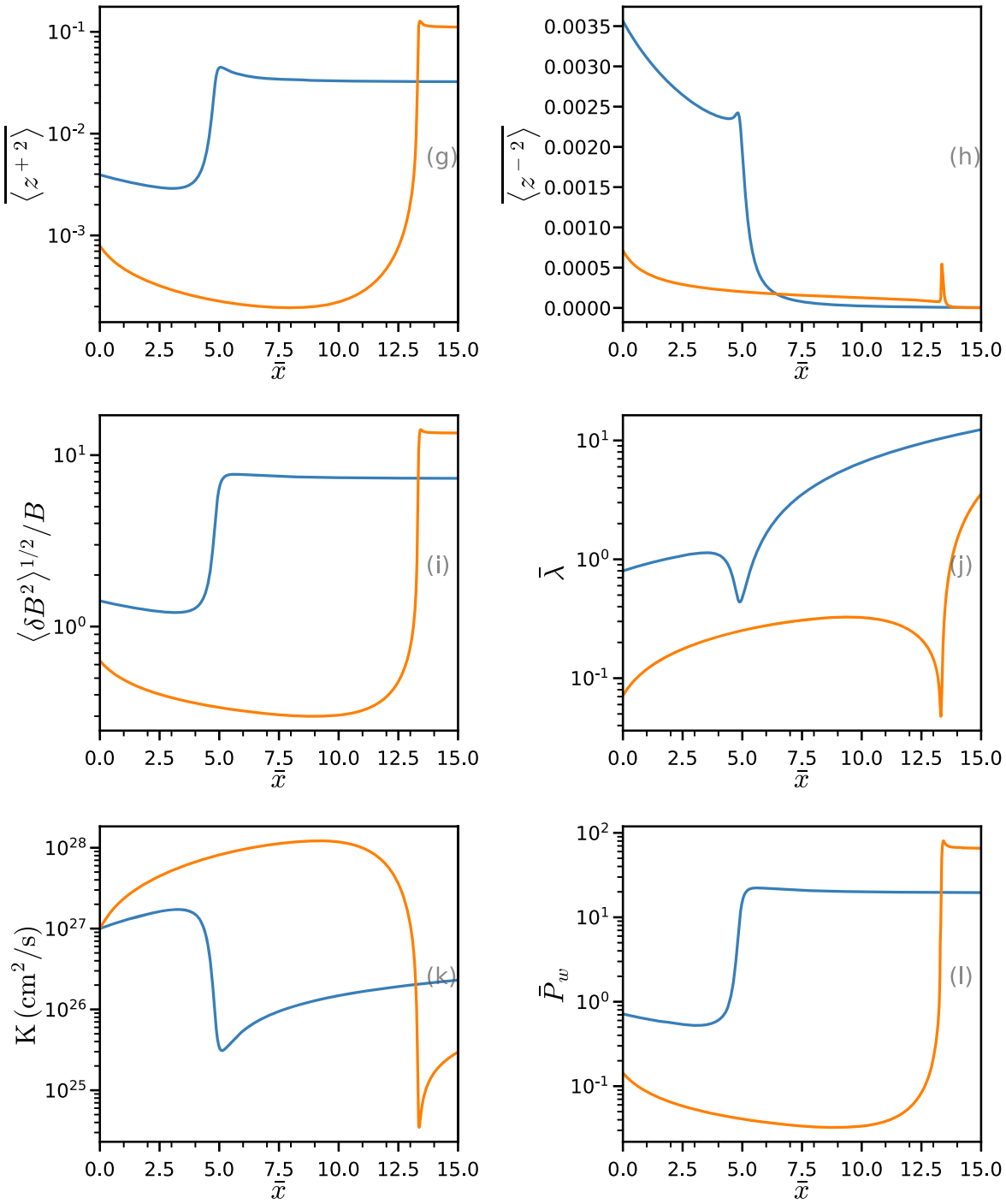

Figure 4. Continuation of Figure 3.

flow, ensuring that the turbulence energy is dominated by the backward propagating modes.

The nature of the turbulence is illustrated in Figure 1(f), which plots the change in the normalized residual energy σ_D with distance. A slight decrease from zero (equal kinetic and magnetic energy densities) to negative (very slightly dominated by the magnetic energy density) is apparent in σ_D far upstream for the orange line. However, for the blue line, σ_D keeps increasing in the far upstream. Then σ_D increases slowly in the upstream region and reaches a maximum value of about 0.17, after which it decreases quickly downstream but remains positive. Being positive indicates that the turbulence kinetic energy exceeds the turbulent magnetic field energy. The ratio of turbulence kinetic energy to turbulence magnetic energy is given by $(1+\sigma_D)/(1-\sigma_D)$, for which the maximum ratio is about 1.41. Interestingly, this is reasonably close to equipartition, as we assumed for the far upstream state.

Figure 2 is a continuation of Figure 1. The normalized energy in backward propagating modes $\langle z^{+2}\rangle$ is illustrated in Figure 2(g). The dissipation of turbulence causes $\langle z^{+2}\rangle$ to decrease from the far upstream value, after which the amplification of turbulence by the gyroresonant streaming instability exceeds the dissipation to generate backward propagating modes efficiently. A small spike structure in

$\langle z^{+2}\rangle$ forms around the shock and then decreases slowly to a constant value downstream.

In contrast, the normalized energy in forward propagating modes $\langle z^{-2}\rangle$ shown in Figure 2(h) is much less than the energy in backward modes. The energy in forward modes $\langle z^{-2}\rangle$ decreases smoothly from the (small) far upstream value until a sharp increase around the shock. Although comparatively large, the increase at the shock is very small when compared with $\langle z^{+2}\rangle$, and strong downstream dissipation decreases the energy immediately after the shock. The positions corresponding to maximum $\langle z^{-2}\rangle$ and $\langle z^{+2}\rangle$ are different by a distance of about 0.15 pc.

The amplitude of the normalized ensemble-averaged magnetic field energy density $\langle \delta B^2\rangle^{1/2}/B$ in turbulent fluctuations is illustrated in Figure 2(i), that is, the ratio of the turbulent magnetic field amplitude to the mean magnetic field amplitude. The ratio is about 0.63 far upstream and decreases slightly with dissipation, before increasing dramatically to a maximum of about 13.89 (14.50) for the blue (orange) solid line. Such a downstream amplification of magnetic turbulence is consistent with observations of $\langle \delta B^2\rangle^{1/2}/B$ downstream of shocks in the heliosphere (e.g., Kallenbach et al. 2005; Zank et al. 2006; Hu et al. 2012; Zank et al. 2021a). The self-generated turbulent magnetic field is much larger than the large-scale magnetic field and the preexisting turbulent magnetic field. The slow decrease downstream is again simply due to the dissipation of turbulence in the absence of driving.

The normalized correlation length $\bar{\lambda}$ shown in Figure 2(j) is an important quantity in determining the rate of dissipation and adjusts itself in response to the strength of turbulence driving in accordance with our assumption that the turbulence is fully developed and governed by Kolmogorov theory. The correlation length also plays an essential role in determining the spatial diffusion coefficient and hence the scattering properties of CRs (Zank et al. 1998; Zhao et al. 2017). The correlation length increases almost linearly from far upstream while dissipation of turbulence dominates, but as the CR-streaming source becomes increasingly important, the correlation length adjusts to increase the rate of dissipation as required by Kolmogorov theory, that is, $\bar{\lambda}$ decreases to make the dissipation terms in Equations (22)–(28) larger. The minimum value of $\bar{\lambda}$ is 0.57 (0.68) for the blue (orange) solid line. Downstream, in the absence of turbulence driving, the correlation length increases with distance as dissipation dominates.

Figure 2(k) illustrates the evolution of the CR diffusion coefficient K. The energy-averaged diffusion coefficient is modeled as $K \propto k_x(x) \propto B^2/\langle \delta B^2(x)\rangle (\lambda(x)/\lambda(0))^{2/3}$. Note the dependence on the turbulent quantities $\delta B^2(x)$ and $\lambda(x)$, both of which are coupled nonlinearly through the Kolmogorov formulation of the turbulence cascade process. Well upstream of the shock, the diffusion coefficient increases slightly as the turbulent magnetic field strength decreases and the correlation length correspondingly increases. The amplification of turbulence upstream of the shock and the decrease in correlation length yield a significant decrease in the diffusion coefficient at the shock. The minimum value of the diffusion coefficient is about 1.36×10^{25} (1.37×10^{25}) $\mathrm{cm}^{-2}\,\mathrm{s}^{-1}$ for the blue (orange) solid line. The downstream increase in the correlation length with the dissipation of turbulence leads to a slow increase of the diffusion coefficient. Energetic particles could be trapped in the transition region.

Finally, Figure 2(l) shows the evolution of the normalized turbulence pressure computed as $\bar{P}_w = P_w/P_{g0} = \frac{\gamma_g M_{s0}^2}{4\bar{U}}\left(\bar{E}_T + \frac{1}{3}\bar{E}_D\right)$. The evolution of turbulence pressure resembles that for the gas pressure and CR pressure. In principle, the turbulence pressure gradient could contribute to the deceleration of the thermal gas. Although the maximum turbulence pressure is slightly larger than the gas pressure, it is only about 15% of the CR pressure at the shock, and thus, the results will not differ much were we to include the turbulence pressure in the dynamical equations governing the CR-mediated system.

The difference between model solutions that assume a prescribed constant diffusion coefficient and those that calculate a self-consistent spatial dependent diffusion coefficient model is apparent—the dashed blue and orange curves versus the solid blue and orange lines. For the constant diffusion coefficient model, all quantities exhibit very wide and smooth profiles, unlike the spatially dependent diffusion coefficient models, which exhibit very narrow and numerically stiff transitions. In the constant diffusion coefficient model, the CR self-generated turbulence only affects the gas pressure through the dissipative heating, whereas in the spatially dependent diffusion coefficient models, the turbulence not only heats the gas but also changes the CR diffusion coefficient. The amplified turbulence reduces the diffusion coefficient and thus leads to an increase in the CR distribution (pressure) spatial gradient. As a consequence, the increase of the CR pressure gradient further results in additional amplification of the turbulence. The resulting CR gradient force becomes so large that it can effectively decelerate the incident gas flow over a very short distance.

3.2. Implications for Observations

In this subsection, we note some general implications of our results for the interpreting of observations of supernova remnants and CR acceleration, avoiding their application to specific cases for the present.

Magnetic field amplification is commonly observed in supernova remnants. The rapid variability of synchrotron emission in several supernova remnants and the presence of narrow X-ray synchrotron rims indicate that the magnetic field is a few tens to a few hundreds μG (Bamba et al. 2005; Uchiyama et al. 2007; Uchiyama & Aharonian 2008; Helder et al. 2012; Vink 2012; Castro et al. 2013). Despite considering a parallel shock, we obtain a downstream magnetic field of about 60 μG, which is far larger than the typical downstream magnetic field resulting from the compression of the interstellar magnetic field by an oblique shock.

The observation of the Hα line at supernova remnant shocks requires that the precursor width be small enough to avoid the complete ionization of neutral hydrogen (Boulares & Cox 1988). The length scale of the precursor is of course set by the CR spatial diffusion coefficient. Upper limits on the CR spatial diffusion coefficient have been estimated to be in the range $\sim 10^{25}$–$2 \times 10^{27}\,\mathrm{cm}^2\,\mathrm{s}^{-1}$ for some Balmer-dominated supernova remnants (Smith et al. 1994; Sollerman et al. 2003; Medina et al. 2014). The investigations of gamma rays from several supernova remnants interacting with molecular clouds found that the diffusion coefficient around the remnant must be less than $\sim 10^{26}\,\mathrm{cm}^2\,\mathrm{s}^{-1}$ (Fujita et al. 2009; Li & Chen 2012).

In our model, we find that a such small diffusion coefficient is a natural consequence of self-generated turbulence by CRs.

4. Conclusion

Despite the by now almost classical status of CR-mediated shocks, the role of fully developed turbulence in determining their steady-state structure has not been addressed properly. For example, McKenzie & Völk (1982) assumed a small-amplitude linear (noninteracting) WKB approximation for Alfvén waves. Here we considered the evolution of turbulence modified by accelerated CRs in the hot ionized interstellar medium by combining a reduced multicomponent fluid model and an incompressible MHD turbulence transport model. The inflowing gas is decelerated by the CR pressure gradient and the CR viscous stress. This removes the need to insert a gas subshock to complete the transition from the upstream to the final downstream state (Mostafavi et al. 2017, 2018). Streaming CRs generate turbulence through a gyroresonant instability, whose growth rate is determined by the CR pressure gradient. The CR pressure gradient is determined in turn by the spatial diffusion coefficient of the CRs, which depends in turn on the turbulence magnetic field energy density and the magnetic field correlation length. This complicated coupling of turbulence and cosmic pressure has not been captured properly in previous investigations of CR-mediated shock structure. We emphasize that the turbulence description used here is not based on a small-amplitude perturbation description but instead corresponds to the decomposition of the turbulence variables into a mean and fluctuating part, from which suitable turbulence "moments" are derived. The turbulence description corresponds therefore to fully developed nonlinear fluctuations, whose couplings are modeled on the basis of Kolmogorov theory (Zank et al. 2012). Besides determining the spatial diffusion coefficient, turbulence dissipation heats the thermal gas, increasing the gas pressure. We numerically solved the self-consistently coupled Equations (1)–(5) and (11)–(14) to obtain the evolution of the relevant physical quantities The model ignores the back reaction of the turbulence pressure, neglects possible "compressible" damping of magnetic field fluctuations via nonlinear Landau damping, and treats the adiabatic index of the CRs as a constant. In future work, we will incorporate these additional possible effects, employ a two-component turbulence transport model for the plasma beta regimes of order 1 or $\ll 1$, extend our model to oblique shocks, and investigate the resulting particle energy spectrum.

We summarize our findings as follows:

1. By including the CR viscosity, we find that the parallel shock requires no discontinuous subshock but instead possesses a smooth transition. By computing the spatial dependent CR diffusion coefficient from the CR streaming self-generated turbulence, we find that the transition is narrow.
2. The gyroresonant instability driven by streaming CRs can amplify the turbulent magnetic field significantly. The magnetic field is completely dominated by the self-generated magnetic field both near the shock front and downstream, being much larger than the background magnetic field.
3. The CR diffusion coefficient is strongly suppressed in the vicinity of the shock and can be three orders smaller in the transition region than far upstream. This has an important dynamical effect on the structure of the shock itself, strongly mediating the CR pressure gradient, which in turn affects the CR streaming instability growth rate.

Understanding the low-frequency turbulence responsible for scattering CRs in the vicinity of interstellar shock waves underlies the physics of diffusive shock acceleration and the interpretation of observations for supernova remnants. This work sheds further light on this important problem.

5. Solutions with a Smaller Diffusion Coefficients Far Upstream

For completeness, we present several cases of CR-mediated turbulent shocks that assume smaller diffusion coefficients far upstream. With $\langle \delta B^2 \rangle / B^2 = 2$ and $\lambda = 0.80$ (model A), or $\langle \delta B^2 \rangle / B^2 = 0.4$ and $\lambda = 0.072$ (model B), the far upstream diffusion coefficient k_0 is 10^{27} cm^2 s^{-1}. All other parameters are fixed to the standard values used in Subection 2.3. The solutions for model A (B), as indicated by blue (orange) solid lines, are summarized in Figures 3 and 4.

Although models A and B use a smaller diffusion coefficient 10^{27} cm^2 s^{-1} than the models of Subsection 2.3, the solutions resemble closely the solutions that use a diffusion coefficient 10^{28} cm^2 s^{-1}. The shock width is about 1.6 pc for model A and 0.2 pc for model B. The minimum diffusion coefficients for models A and B are 3.1×10^{25} cm^2 s^{-1} and 3.5×10^{24} cm^2 s^{-1}, respectively. The maximum ratio of the turbulence magnetic energy and the background magnetic field is about 8 and 14 for models A and B, respectively. All the results presented in Figures 3 and 4 are fully consistent with our conclusions above.

We acknowledge the partial support of an NSF EPSCoR RII-Track-1 Cooperative Agreement OIA- 244 1655280, partial support from a NASA LWS grant 80NSSC20K1783, and partial support from a NASA IMAP subaward under NASA contract 80GSFC19C0027.

ORCID iDs

B.-B. Wang https://orcid.org/0000-0002-6000-1262
G. P. Zank https://orcid.org/0000-0002-4642-6192
L.-L. Zhao https://orcid.org/0000-0002-4299-0490
L. Adhikari https://orcid.org/0000-0003-1549-5256

References

Adhikari, L., Zank, G. P., Bruno, R., et al. 2015, ApJ, 805, 63
Adhikari, L., Zank, G. P., Hunana, P., & Hu, Q. 2016, ApJ, 833, 218
Adhikari, L., Zank, G. P., & Zhao, L. L. 2021, Fluids, 6, 368
Amato, E., & Blasi, P. 2009, MNRAS, 392, 1591
Axford, W. I., Leer, E., & McKenzie, J. F. 1982, A&A, 111, 317
Bamba, A., Yamazaki, R., Yoshida, T., Terasawa, T., & Koyama, K. 2005, ApJ, 621, 793
Beck, R., Brandenburg, A., Moss, D., Shukurov, A., & Sokoloff, D. 1996, ARA&A, 34, 155
Bell, A. R. 1978, MNRAS, 182, 147
Bell, A. R. 2004, MNRAS, 353, 550
Blandford, R., & Eichler, D. 1987, PhR, 154, 1
Blasi, P. 2013, A&ARv, 21, 70
Boulares, A., & Cox, D. P. 1988, ApJ, 333, 198
Castro, D., Lopez, L. A., Slane, P. O., et al. 2013, ApJ, 779, 49
De La Torre Luque, P., Mazziotta, M. N., Loparco, F., Gargano, F., & Serini, D. 2021, JCAP, 2021, 010
Dosch, A., Adhikari, L., & Zank, G. P. 2013, in AIP Conf. Ser. 1539, Solar Wind 13, ed. G. P. Zank et al. (Melville, NY: AIP), 155
Drury, L. O. 1983, RPPh, 46, 973
Drury, L. O., & Völk, J. H. 1981, ApJ, 248, 344

Evoli, C., Aloisio, R., & Blasi, P. 2019, PhRvD, 99, 103023
Fujita, Y., Ohira, Y., Tanaka, S. J., & Takahara, F. 2009, ApJL, 707, L179
Haverkorn, M., Brown, J. C., Gaensler, B. M., & McClure-Griffiths, N. M. 2008, ApJ, 680, 362
Haverkorn, M., Katgert, P., & de Bruyn, A. G. 2004, A&A, 427, 169
Haverkorn, M., & Spangler, S. R. 2013, SSRv, 178, 483
Helder, E. A., Vink, J., Bykov, A. M., et al. 2012, SSRv, 173, 369
Hindmarsh, A. C., Brown, P. N., Grant, K. E., et al. 2005, Atoms, 31, 363
Hu, Q., Ao, X., Peltzer, R., & Zank, G. P. 2012, in AIP Conf. Ser. 1500, Space Weather: the Space Radiation Environment: XI Annual International AstroPhysics Conference, ed. Q. Hu et al. (Melville, NY: AIP), 192
Jones, F. C., & Ellison, D. C. 1991, SSRv, 58, 259
Kallenbach, R., Bamert, K., Hilchenbach, M., & Smith, C. W. 2005, in AIP Conf. Ser. 781, The Physics of Collisionless Shocks: IV Annual IGPP International Astrophysics Conference, ed. G. Li, G. P. Zank, & C. T. Russell (Melville, NY: AIP), 129
Lerche, I. 1967, ApJ, 147, 689
Li, H., & Chen, Y. 2012, MNRAS, 421, 935
Malkov, M. A., & Drury, L. O. 2001, RPPh, 64, 429
McKenzie, J. F., & Völk, H. J. 1982, A&A, 116, 191
Medina, A. A., Raymond, J. C., Edgar, R. J., et al. 2014, ApJ, 791, 30
Minnie, J., Bieber, J. W., Matthaeus, W. H., & Burger, R. A. 2007, ApJ, 663, 1049
Minter, A. H., & Spangler, S. R. 1997, ApJ, 485, 182
Miville-Deschênes, M. A., Ysard, N., Lavabre, A., et al. 2008, A&A, 490, 1093
Mostafavi, P., & Zank, G. P. 2018, ApJL, 854, L15
Mostafavi, P., Zank, G. P., & Webb, G. M. 2017, ApJ, 841, 4
Mostafavi, P., Zank, G. P., & Webb, G. M. 2018, ApJ, 868, 120
Mostafavi, P., Zank, G. P., Zirnstein, E. J., & McComas, D. J. 2019, ApJL, 878, L24
Rackauckas, C., & Nie, Q. 2017, JORS, 5, 1
Shalchi, A. 2009, APh, 31, 237
Shiota, D., Zank, G. P., Adhikari, L., et al. 2017, ApJ, 837, 75
Smith, R. C., Raymond, J. C., & Laming, J. M. 1994, ApJ, 420, 286
Snodin, A. P., Shukurov, A., Sarson, G. R., Bushby, P. J., & Rodrigues, L. F. S. 2016, MNRAS, 457, 3975
Sollerman, J., Ghavamian, P., Lundqvist, P., & Smith, R. C. 2003, A&A, 407, 249
Uchiyama, Y., & Aharonian, F. A. 2008, ApJL, 677, L105
Uchiyama, Y., Aharonian, F. A., Tanaka, T., Takahashi, T., & Maeda, Y. 2007, Natur, 449, 576
Vink, J. 2012, A&ARv, 20, 49
Völk, H. J., Drury, L. O., & McKenzie, J. F. 1984, A&A, 130, 19
Wang, B. B., Zank, G. P., Adhikari, L., & Zhao, L. L. 2022, ApJ, 928, 176
Webb, G. M., Zank, G. P., Kaghashvili, E. K., & le Roux, J. A. 2006, ApJ, 651, 211
Zank, G. P. 2016, GSL, 3, 22
Zank, G. P., Adhikari, L., Hunana, P., et al. 2017, ApJ, 835, 147
Zank, G. P., Adhikari, L., Zhao, L. L., et al. 2018, ApJ, 869, 23
Zank, G. P., Dosch, A., Hunana, P., et al. 2012, ApJ, 745, 35
Zank, G. P., Hunana, P., Mostafavi, P., & Goldstein, M. L. 2014, ApJ, 797, 87
Zank, G. P., Li, G., Florinski, V., et al. 2006, JGRA, 111, A06108
Zank, G. P., Li, G., Florinski, V., et al. 2004, JGRA, 109, A04107
Zank, G. P., & Matthaeus, W. H. 1993, PhFlA, 5, 257
Zank, G. P., Matthaeus, W. H., Bieber, J. W., & Moraal, H. 1998, JGR, 103, 2085
Zank, G. P., Nakanotani, M., Zhao, L. L., et al. 2021a, ApJ, 913, 127
Zank, G. P., Zhao, L. L., Adhikari, L., et al. 2021b, PhPl, 28, 080501
Zhao, L. L., Adhikari, L., Zank, G. P., Hu, Q., & Feng, X. S. 2017, ApJ, 849, 88
Zhao, L. L., Adhikari, L., Zank, G. P., Hu, Q., & Feng, X. S. 2018, ApJ, 856, 94
Zweibel, E. G. 2017, PhPl, 24, 055402
Zweibel, E. G., & McKee, C. F. 1995, ApJ, 439, 779